Properties of Small Molecules Affecting Insulin Receptor Function

Morten Schlein,* Svend Ludvigsen, Helle B. Olsen, Asser S. Andersen, Gillian M. Danielsen, and Niels C. Kaarsholm

Health Care Discovery, Novo Nordisk A/S, Novo Alle 1, DK-2880 Bagsvaerd, Denmark

Received August 10, 2001; Revised Manuscript Received September 14, 2001

ABSTRACT: Small molecules with insulin mimetic effects and oral availability are of interest for potential substitution of insulin injections in the treatment of diabetes. We have searched databases for compounds capable of mimicking one epitope of the insulin molecule known to be involved in binding to the insulin receptor (IR). This approach identifies thymolphthalein, which is an apparent weak agonist that displaces insulin from its receptor, stimulates auto- and substrate phosphorylation of IR, and potentiates lipogenesis in adipocytes in the presence of submaximal concentrations of insulin. The various effects are observed in the 10^{-5}−10^{-3} M range of ligand concentration and result in partial insulin activity. Furthermore, analogues of the related phenol red and fluorescein molecules fully displace insulin from the IR ectodomain, however, without insulin agonistic effects. The interactions are further characterized by NMR, UV−vis, and fluorescence spectroscopies. It is shown that both fluorescence and UV−vis changes in the ligand spectra induced by IR fragments occur with K_d values similar to those obtained in the displacement assay. Nevertheless, insulin itself cannot completely abolish binding of the small molecules. Determination of the binding stoichiometry reveals multiple binding sites for ligands of which one overlaps with the insulin binding site on the receptor.

Molecular mimicry of peptide hormones and cytokines has potential applications for the substitution of injected protein pharmaceuticals with orally available compounds. In recent years, a few examples of peptides or small molecules mimicking protein hormones or cytokines in an agonistic manner have emerged (*1*−*5*). These molecules (or their parent compounds) are usually found by screening different kinds of large and diverse libraries using biochemical and biological assays.

The insulin−insulin receptor (IR)[1] system is an attractive target for small molecule mimicry. When the protein hormone binds to the extracellular part of its receptor, a signaling cascade is initiated that ultimately results in a wide range of biological effects including uptake of glucose by target cells (*6*). The intrinsic binding event is thought to induce a conformational change in the receptor that leads to activation of the intracellular tyrosine kinase domain (*7*−*9*). The insulin mimetics known today elicit their effects by interacting with molecules other than IR (*10*−*12*) or by interaction with IR by some means other than binding to the hormone binding site (*13*−*18*).

The insulin molecule is structurally well characterized, and biological potency data are available for numerous engineered or naturally occurring insulin variants (e.g., *19*). Nevertheless, because no atomic structures exist of IR in the presence or absence of bound ligand, little is known about the events immediately following insulin binding. The IR molecule is a heterotetramer consisting of two α−β dimers (*20*). Disulfide bridges connect the α and the β subunits within the dimer as well as the β subunits of α−β dimers within the tetramer (*21*). The α subunit is extracellular and provides the insulin binding site. The β subunit contains a short extracellular region, a transmembrane segment, and an intracellular tyrosine kinase domain. High-resolution structural information is available for the catalytic core of the tyrosine kinase domain in its inactive and active conformations (*7*, *22*) and for a nonbinding fragment of the ectodomain from the homologous IGF-1 receptor (*23*).

Rational design of molecular mimicry at the intrinsic hormone binding site is challenging due to the lack of structural information on the insulin−IR complex and due to the shape and large extent of the putative molecular surfaces involved in the recognition process. Nevertheless, targeting the first event in the signal transduction pathway may be preferable to attain full and specific mimetic effect. As a supplement to random screening of libraries, we have used structure−function analysis of insulin based on crystal and NMR structures of hexameric and monomeric insulins (*19*, *24*−*27*) as a starting point in the search for putative

* Corresponding author: Dr. Morten Schlein, Health Care Discovery, Novo Nordisk A/S, Novo Alle 6BS.90, DK-2880 Bagsvaerd, Denmark, Phone: +45 4442 6146, fax: +45 4444 4256, E-mail: mosc@novonordisk.com.

[1] Abbreviations: Abs, absorption; ACD, Available Chemicals Database; BSA, bovine serum albumin; DMSO, dimethyl sulfoxide; EDTA, ethylenediaminetetraacetate; ELISA, enzyme-linked immunosorbent assay; ECL, enhanced chemiluminescence; EO, eosin; ER, erythrosine; hIR, human insulin receptor; HSA, human serum albumin; IGF-1, insulin-like growth factor 1; IgG, immunoglobulin G; IR, insulin receptor; IRS-1, human insulin receptor substrate 1; mIR, minimized insulin receptor comprising residues 1−468 and 704−717 of the α-subunit; NOE, nuclear Overhauser effect; NOESY, nuclear Overhauser effect spectroscopy; PDB, Protein Databank; PVDF, poly(vinylidene difluoride); SD, standard derivation; SDS, sodium dodecyl sulfate; SEM, standard error of the mean; sIR, soluble IR comprising residues 1−917 (without exon 11) of hIR; sIRFc, sIR fused to the Fc domain from IgG; TP, thymolphthalein; UV−vis, ultraviolet−visible.

10.1021/bi015672w CCC: $20.00
Published on Web 10/20/2001

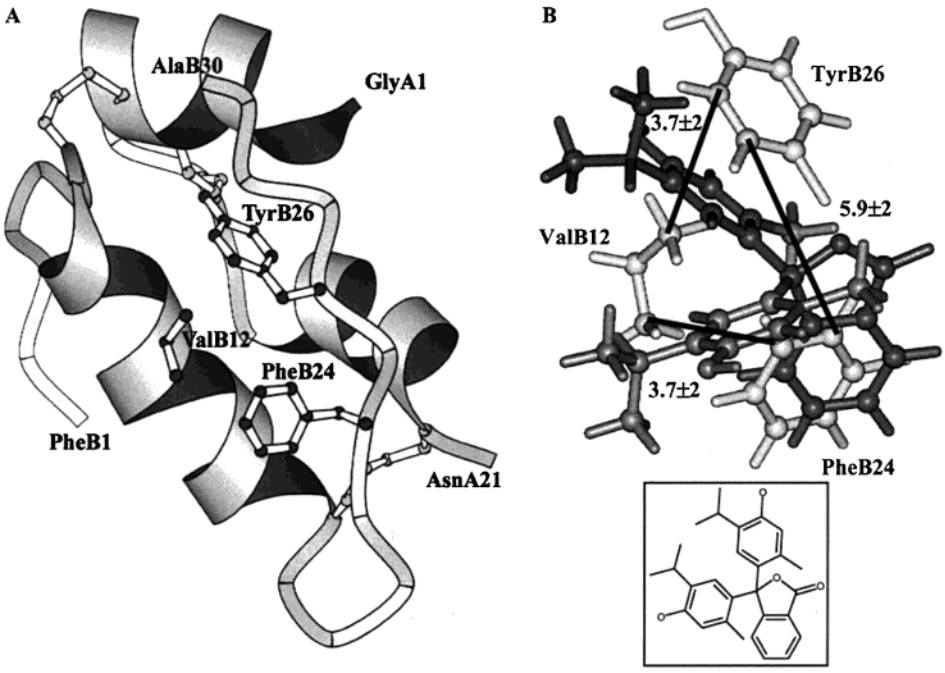

FIGURE 1: (A) The insulin molecule (1hls.pdb). The ValB12, PheB24, and TyrB26 epitope is shown in ball-and-stick representation. (B) The database search hit thymolphthalein (TP, structure shown as insert) superimposed on the ValB12, PheB24, and TyrB26 epitope (shown in white). The parts of TP fitting to the search query are shown in dark gray, and the remaining parts are in light gray. Arbitrary defined distances with tolerances between atoms in the search query are shown in black.

small molecule ligands for the insulin receptor. This approach is based on the assumption that the selected epitopes on the insulin molecule constitute so-called functional epitopes or "hot spots", i.e., they provide the majority of the binding energy in the protein−protein interface similar to what has been found in the human growth hormone−human growth hormone receptor complex (*28*). Given the right structural context, such small molecules mimicking hot spots may in principle interfere with (and most likely antagonize) the hormone−receptor recognition event.

In the present work, we use the structure of the insulin epitope comprising residues ValB12, PheB24, and TyrB26 as a starting point for identifying molecules in the Available Chemicals Database (ACD) that may display a similar three-dimensional configuration. These residues form a hydrophobic patch on the insulin surface (see Figure 1A), which is known to be important for the binding to the insulin receptor (*26* and references therein). We show herein that several hits from the database searches indeed affect insulin−receptor interactions in one or more functional assays including the displacement of insulin from the insulin receptor, the autophosphorylation of (or the substrate phosphorylation by) the holoreceptor, and glucose uptake and incorporation into lipid in isolated primary mouse adipocytes. In the various assays, the effects are typically observed at ligand concentrations in the range of 10^{-5}−10^{-3} M. For a selection of ligands with appropriate chromophoric properties, we further employ a variety of spectroscopic techniques to characterize the receptor interaction in detail. It is shown that these ligands typically bind to the insulin receptor in several modes of which some, but not all, are directly competitive with the binding of the native hormone.

MATERIALS AND METHODS

Molecular Modeling and Database Search. Molecular modeling was done using the Sybyl version 6.5 program package (Tripos Inc., St. Louis, USA). Coordinates for the atoms describing the chemical moieties in the selected insulin epitope were extracted from an insulin PDB file (1hls.pdb). The "3DB Unity" utility in the Sybyl program package was used to define distances between a number of the extracted atoms. Tolerances were applied to these distances to give a reasonable number of hits (and indirectly to take conformational changes and uncertainties of the protein structure into account). The tolerances were often rather large, up to 50% of the distance itself. This was used as a query for searching in ACD. The search algorithm initially identified a set of molecules that contain at least those chemical moieties present in the query. Next, the program selected those molecules, which have the common chemical moieties within the distances, defined in the search query. An example of a database hit superimposed on the search query is shown in Figure 1B. Approximately 20 molecules were selected from this initial search.

Database searches using two-dimensional structures for commercially available compounds and analogues were performed using Isis/Base version 2 (MDL Information Systems Inc., San Leandro, USA) in the ACD. All versions of software and databases were the latest available at the given time in the period of 1997−2000.

All chemicals were purchased from Sigma Chemicals (St. Louis, USA), Aldrich (Milwaukee, USA), or Fluka (Milwaukee, USA).

Selected stock solutions of the molecules were tested in an ELISA assay for insulin contamination and no insulin was found in the samples.

Plots of protein structures were produced using the Molscript program (*29*).

Displacement Assay. The displacement assay was performed as described (*30*, *31*) with the soluble IR (sIR) (*32*) fused to the Fc domain from IgG (resulting construct called sIRFc). Binding reactions in each well were 100 μL,

containing 40 pM [^{125}I]-(TyrA14)-human insulin, test compound, and 2% dimethyl sulfoxide (DMSO). Control samples containing only DMSO or human insulin and DMSO in final concentrations of 2% and 100 nM, respectively, were included in each series. Binding data were analyzed using nonlinear regression in GraphPad Prism 3.01 (GraphPad Software, San Diego, USA) and eq 1.

$$\Delta = \frac{\Delta_{max}}{1 + 10^{\log[\text{competitor}] - \log EC50}} \quad (1)$$

Δ_{max} and Δ are the radioactivities bound in absence and presence of a given [competitor]. EC50 is the [competitor] needed to displace 50% of the tracer binding. Since [tracer] $\ll K_d$, the determined EC50 equals the dissociation constant for the inhibitor−receptor interaction (*33*).

Autophosphorylation. Baby hamster kidney cells were used for overexpressing human IR (hIR), and the crude extract was partially purified over a wheat germ agglutinin column. In each sample, 5 μL of partially purified hIR in 0.1% Triton X-100 was mixed with 5 μL of 4× APB (200 mM Tris pH 7.5, 40 mM $MgCl_2$, 6 mM $MnCl_2$, 200 μM $NaVO_3$, 0.2 mg/mL BSA) and 5 μL of test compound in 8% DMSO. Samples were incubated at room temperature for 1 h before addition of 5 μL of 10 μM ATP. The reactions were stopped after 10 min by addition of 7 μL of 4× SDS loading buffer. Samples were run on a 10% Bis-Tris SDS gel with MOPS running buffer (Nupage, Novex), and the gel was electroblotted onto a PVDF membrane (Novex). The blot was blocked in TBS (10 mM Tris pH 7.5, 150 mM NaCl) with 2% BSA overnight at 4 °C and then incubated with an anti-phosphotyrosine antibody−horseradish peroxidase conjugate (Transduction Laboratories #RC20:HRPO) diluted 1:2000 in TBST (TBS with 0.1% Tween) for 1 h at room temperature. After three washes with TBST, the bound antibodies were detected by enhanced chemiluminescence (ECL, Amersham Pharmacia Biotech) and visualized using a Luminescent Image Analyzer CCD camera (Fujifilm, LAS-1000) with Image Gauge version 2.53 software (Fujifilm).

Substrate Phosphorylation Assay. The substrate phosphorylation assay utilizes the peptide KSRGDYMTMQIG where positions 2−10 correspond to the sequence flanking Tyr989 in IRS-1. The N-terminal Lys is biotinylated. Samples of 100 μL were prepared in microtiter plates (Falcon #3912) and contained 50 ng of hIR, 50 mM Tris, pH 7.5, 10 mM $MgCl_2$, 1.5 mM $MnCl_2$, 50 μM $NaVO_3$, 50 μg/mL BSA, 0.025% Triton X-100, 12.5 μM ATP, 2 μg/mL biotinylated peptide substrate, 2% DMSO, and appropriate concentration of test compound. After 1 h incubation at room temperature, 10 μL of 200 mM EDTA was added to each well, and the contents were transferred to streptavidin coated microtiter plates (Nunc, #236001) for 1 h incubation. The plates were washed three times with TBST before addition of 100 μL of anti phosphotyrosine antibody−horseradish peroxidase conjugate diluted 1:2000 in TBST. After 30 min and washing with TBST, 100 μL of TMB-one peroxidase substrate (Kem En Tech, Denmark) was added to each well. The enzymatic reaction was stopped with 10 μL of 10% H_2SO_4 when an appropriate intensity of blue coloring had developed (approximately 10−15 min). Finally, the formation of phosphotyrosines was quantified by measuring the absorption at 450 nm in each well using a Multiskan RC plate reader (Labsystems).

Glucose Incorporation into Lipid. Determination of ^{3}H-glucose incorporation into lipid in mouse epididymal adipocytes was adapted from the method of Moody et al. (*34*). Briefly, epididymal fat pads were dissected from B6D2F1 mice (Charles River, Germany) and minced, and adipocytes were prepared by collagenase degradation during shaking for 1.5 h, at 36 °C in 110 mM NaCl, 5 mM KCl, 1.2 mM KH_2PO_4, 1.2 mM $MgSO_4$, 2.5 mM $CaCl_2$, 25 mM Hepes, pH 7.9, 4% HSA, 1.1 mM glucose, and 0.4 mg/mL collagenase type 1 (Worthington Biochemical Corporation). Cells were then filtered through two layers of gauze and centrifuged for several seconds at 500*g*. Cells were then washed twice (110 mM NaCl, 5 mM KCl, 1.2 mM KH_2PO_4, 1.2 mM $MgSO_4$, 2.5 mM $CaCl_2$, 25 mM Hepes, pH 7.9, 1% HSA), and 100 μL aliquots pipetted into 96 well Picoplates (Packard). A total of 10 μL of insulin and 10 μL of compound or control solvent was added, and the assay initiated by the addition of 10 μL of D-(3-^{3}H)glucose and glucose to a final concentration of 0.5 mM glucose. The plates were shaken for 1.5 h, and the assay was stopped by the addition of MicroScint-E (Packard). Plates were counted in a TopCount (Packard). Full insulin dose responses were run on all plates. To exclude technical interference of the compounds, controls were performed with maximal insulin alone, and after stopping with MicroScint-E, compound was added to 100 μM prior to counting.

Spectroscopy. The insulin receptor constructs sIR and the minimized IR (mIR) were produced and purified as described previously (*9*, *31*, *35*).

NMR spectra were recorded on a 600 MHz Varian Inova instrument basically according to ref *24* and references therein. The mixing time for NOESY spectra was 500 ms. Final sample concentrations were 2 mM eosin (EO), 2% ^{2}H-DMSO, 100 mM ^{2}H-Tris, pH 8, 100 mM NaCl, 10 mM $MgCl_2$, 10% ^2H_2O.

UV−vis spectra were recorded on a Kontron Uvikon 922 double beam or a Hewlett-Packard HP8453 diode array spectrophotometers. Protein concentrations were estimated using calculated extinction coefficients at 280 nm (*36*). A typical titration experiment was carried out by adding ligand, appropriately diluted in buffer from a 100 mM solution in DMSO, to samples containing receptor and buffer only, respectively. The total addition of ligand contributed less than 5% to the total volume. All spectra were corrected for slight baseline drift before the difference spectra were calculated mathematically as (sample with receptor) − (sample with buffer). Alternatively, each concentration of ligand was mixed with either receptor or buffer in a sample. A one-site binding equation was fitted to the spectroscopic change, Δ, and the ligand concentration, [L] (eq 2):

$$\Delta = \Delta_{max} \frac{[L]}{[L] + K_d} \quad (2)$$

Note that the displacement/competition experiments employ the insulin mutant HisB10Asp, ProB28Asp modified in the monomer/monomer interface to avoid complications arising from insulin dimerization in solution (*37*).

Fluorescence intensities were recorded with a Perkin-Elmer LS-50B Luminescence spectrometer. All spectra were ob-

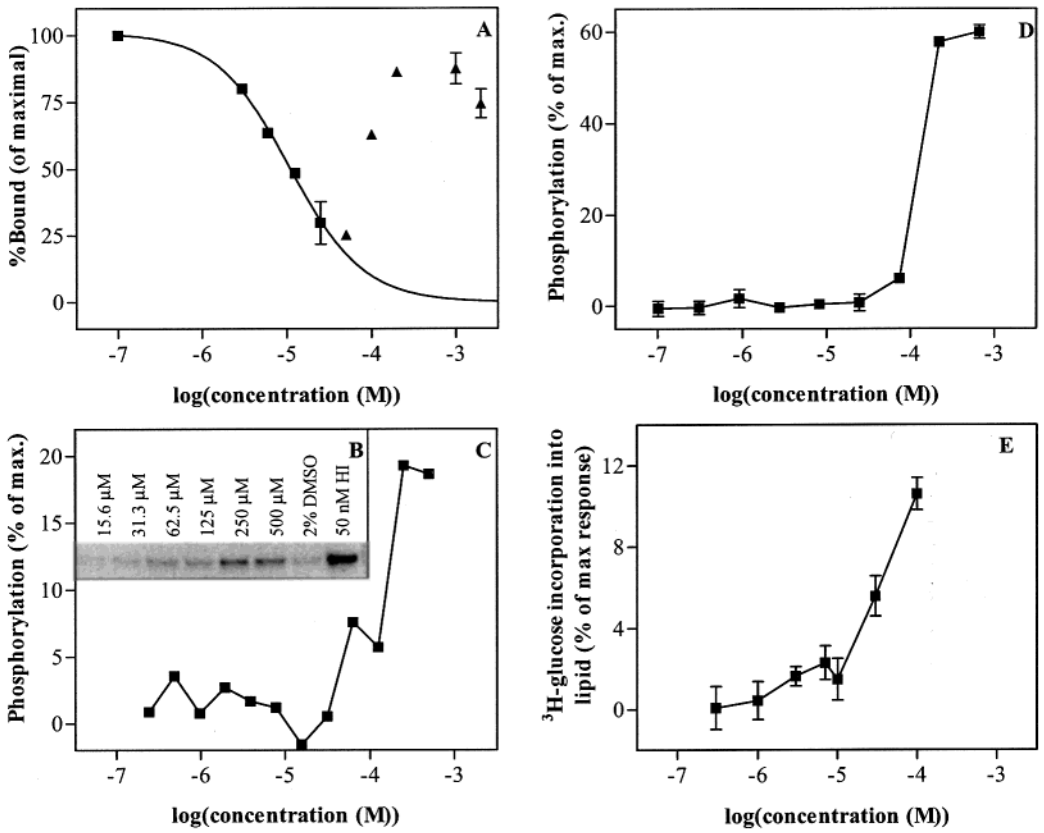

FIGURE 2: Interaction between TP and IR. (A) Displacement of ^{125}I-insulin from sIRFc by TP. Full line is one-site competition curve (eq 1) fitted to the data points shown as squares yielding $K_d = 10\ \mu M \pm 1$. The rest of the dataset is shown as triangles. All data points are mean of duplicate samples and shown with SEM bars. (B) Western blot showing autophosphorylation of hIR β subunits in the presence of 50 nM human insulin, 2% DMSO, or increasing TP concentration. (C) Quantization of full range of TP concentrations shown in panel B. The data are normalized using the value of the 2% DMSO as 0% and that of 50 nM human insulin as 100%. (D) Substrate phosphorylation by hIR in the presence of increasing TP concentration. The data are normalized as in panel C. All data points are mean of duplicate samples and shown with SEM bars. (E) ^{3}H-glucose incorporation into lipid. Insulin is added to cell suspensions to give approximately 15% of full insulin activity. The graph shows the increase in activity on addition of TP. Individual experiments were run with triplicate determinations. Data points show the average of three experiments, ± SEM.

tained using a light path of 0.5 cm and corrected for background emission of the buffer. Erythrosine emission spectra were obtained by excitation at 470 nm. Both excitation and emission slit widths were 5 nm. Titration experiments were carried out as described for absorption spectroscopy.

The binding stoichiometry was determined using the continuous variation method (*38*). Samples contained a total concentration of receptor and ligand of 86 μM, while the mole fractions of the two were varied, in the presence of 100 mM Tris, pH 7.8, 100 mM NaCl, and 10 mM $MgCl_2$. When appropriate, insulin HisB10Asp ProB28Asp was present at 80 μM. Difference absorption spectra were obtained as described above using a 0.02 cm cuvette. To improve the signal-to-noise ratio, the difference between the two extremes of ΔAbs was calculated (*39*) and plotted against the mole fraction of mIR. Tangents to this curve were drawn through $x = 0$ and $x = 1$, and the mole fraction x_s at their intersect was used to calculate the stoichiometry, n, using eq 3 (*40*):

$$n = \frac{1 - x_s}{x_s} \tag{3}$$

RESULTS

A Weak Insulin Agonist Identified from the Extracted Epitope Search. Among the hits from the database search using the ValB12, PheB24, and TyrB26 coordinates, one molecule exhibits weak insulin agonistic effects. Thymolphthalein (TP, see Figure 1B) displaces radioactively labeled insulin from sIRFc with a valley shaped concentration dependence as shown in Figure 2A. At [TP] values up to 100 μM, about 70% of the bound insulin is displaced with a one-site competition curve corresponding to $K_d = 10\ \mu M$. At higher [TP], this effect diminishes until TP eventually precipitates in the sample buffer.

Addition of TP also stimulates about 15% increase in autophosphorylation of the full-length human insulin receptor (hIR) (Figure 2B,C). The effect is observed in the 100 μM−1 mM TP concentration range. In the same range, an increase in substrate phosphorylation in the presence of TP is also observed (Figure 2D).

At an insulin level resulting in approximately 15% of maximal insulin stimulation, ^{3}H-glucose incorporation into lipid in primary mouse adipocytes is further increased by approximately 10% in the presence of 100 μM TP (10.6% ± 1.4% SD, $n = 3$), see Figure 2E. In the absence of insulin, no effect was observed.

Interestingly, the activation effects (Figure 2B−E) occur in the same concentration range corresponding to the right branch of the valley shaped TP displacement curve (Figure 2A). This phenomenon was not further explored in the present study.

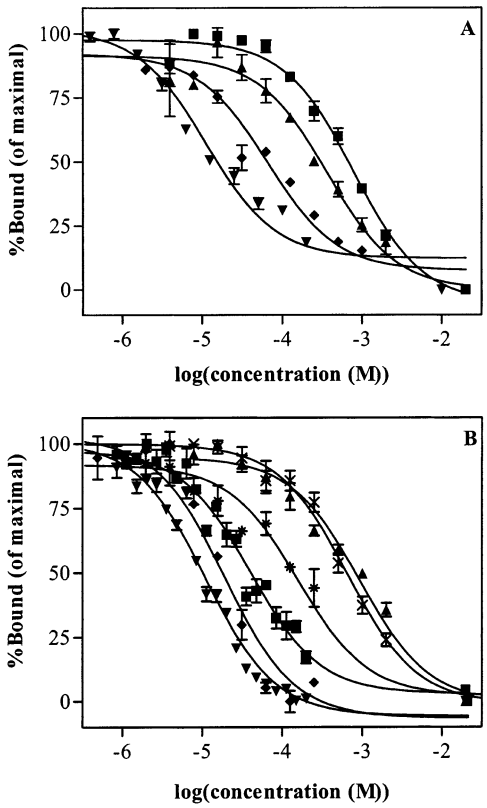

FIGURE 3: Displacement of ^{125}I-insulin from sIRFc by phenol red and fluorescein derivatives. Full lines are one-site competition curves (eq 1) fitted to the data points. See Table 1 for structures, abbreviations, and representative K_d values. (A) Phenol red (■), bromophenol red (▲), bromophenol blue (◆), and iodophenol blue (▼). (B) Fluorescein (▲), gallein (×), tetrachlorofluorecein (∗), EO (■), rose bengal (◆), and ER (▼). All data points are mean of triplicate (EO and ER) or duplicate samples and shown with SEM bars.

Displacement of Insulin from sIRFc by Fluorescein and Phenol Red Analogues. A second round of database search was performed aiming at identification of TP analogues with increased insulin agonistic effect. TP belongs to the phenolphthalein class of acid−base indicators. A substructure search was done in ACD using phenolphthalein as a query to identify all molecules containing this motif. The hits included different derivatives of phenolphthalein with an ether bridge between the two phenolic rings (e.g., fluorescein). A similar search was performed using phenol red as a substructure search query. This molecule is closely related to phenolphthalein, in that the carboxylic acid group is replaced by a sulfonic acid group.

From the database searches, approximately 100 derivatives of the two queries and molecules with similarity to the queries were selected and tested for binding to sIRFc in a displacement assay. In contrast to TP, many compounds exhibit full one-site competition curves with complete displacement of the labeled insulin, see Figure 3 and Table 1. However, some compounds (e.g., thymol blue) exhibit a steeper displacement curve, indicating either multiple, different or interacting binding sites. The measured K_d values are in the 10 μM−1 mM range and reveal a simple structure−activity relationship for the binding of these two classes of compounds to sIRFc. Addition of halogen atoms in the ortho positions on the phenolic rings clearly increases binding affinity. The effect is larger with two rather than one halogen substituent on each ring (e.g., bromophenol red versus bromophenol blue, Figure 3A), and the effect is larger with I than Br (e.g., erythrosine (ER) versus eosin (EO), Figure 3B). This trend is observed both for fluorescein and phenol red derivatives and demonstrates a distinct hydrophobic contribution to the binding interaction in this context.

Table 1: Molecules Identified in the Second Database Search and Their K_d Values ± SD for Displacement of Insulin from SIRFc

	K_d[a]/μM		K_d[a]/μM
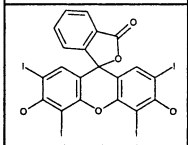 Erythrosine (ER)	11 ± 1	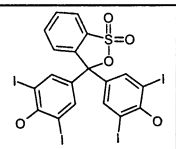 Iodophenol blue	11 ± 2
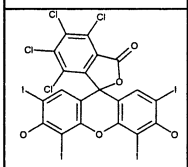 Rose Bengal	20 ± 4	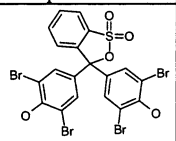 Bromophenol blue	65 ± 11
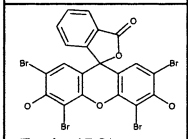 Eosin (EO)	40 ± 4	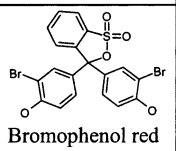 Bromophenol red	360 ± 65
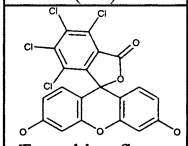 Tetrachlorofluo-rescein	160 ± 30	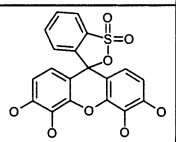 Pyrogallol red	640 ± 100
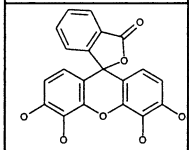 Gallein	650 ± 72	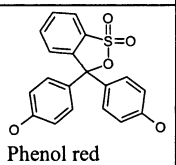 Phenol red	780 ± 100
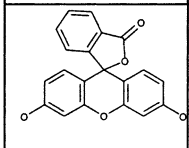 Fluorescein	900 ± 125	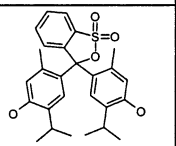 Thymol blue	> 1000

[a] The K_d values are representative for multiple experiments with duplicate or triplicate samples.

In contrast with TP, all molecules from the second database search exhibit either antagonistic or no effect when tested in the autophosphorylation assay. EO inhibits the autophosphorylation of hIR with $K_d = 7\ \mu M \pm 2$ (data not shown), as compared to $K_d = 40\ \mu M$ for sIRFc binding as determined in the displacement assay.

NMR Investigations of EO−mIR Interaction. The binding of EO to mIR was examined by NMR. A ^{1}H 2D NOESY NMR spectrum was acquired of 2 mM EO in the absence

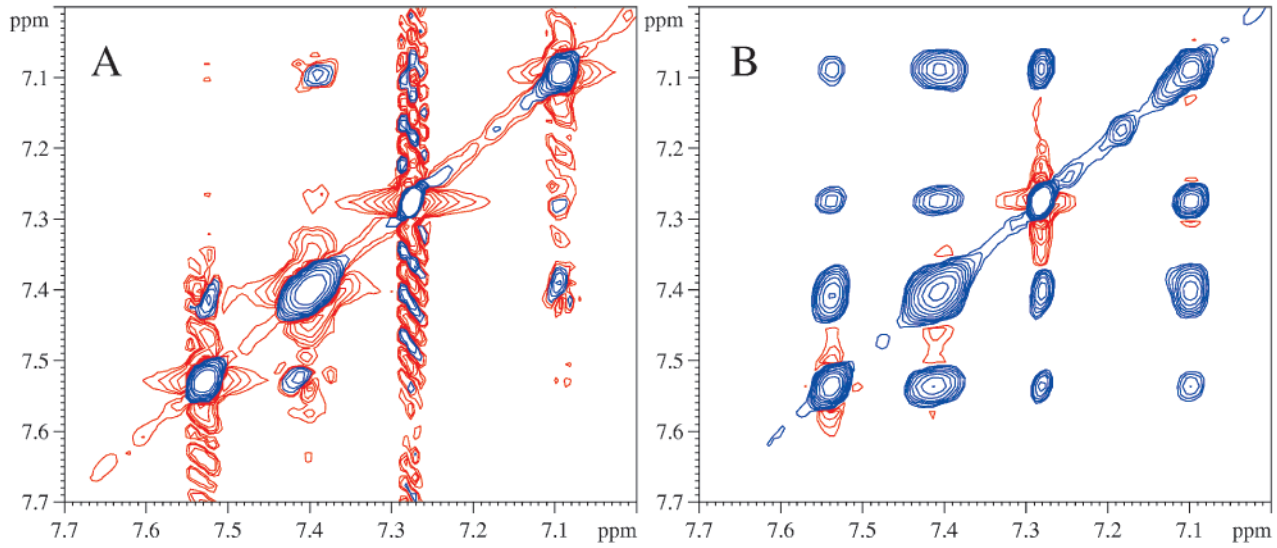

FIGURE 4: Transferred NOESY cross-peaks in the EO spectrum induced by mIR. The ^{1}H 2D NOESY spectrum of 2 mM EO in the absence (A) and presence of 10 μM mIR (B). Negative contours are colored red, and positive are colored blue.

and presence of 10 μM mIR. These conditions are optimized for the appearance of transferred NOE cross-peaks, in case the K_d, and hence k_{off} value allows detection of such. Transferred NOE cross-peaks are indeed observed by comparison of the two spectra, see Figure 4: The spectrum of EO alone has few, mostly negative cross-peaks. In contrast, the presence of a low [mIR] results in the appearance of more cross-peaks, all of which are relatively intense and of positive sign as the diagonal signals. Note also that the ripples in the spectrum of EO alone, caused by a truncation effect due to narrow line widths of the signals, are gone in the presence of mIR indicative of signal broadening. This is a consequence of the slower tumbling of the EO molecules when bound to mIR. These data clearly show that EO binds to mIR.

Binding of EO and ER to sIR and mIR Measured by UV−vis and Fluorescence Spectroscopy. Initial spectroscopic measurements of ligand binding in solution were performed using sIR. This makes comparison with the displacement assay, using sIRFc, possible. The presence of sIR induces changes in the EO absorption spectrum and a decrease at 510 nm fits eq 2 with $K_d = 24\ \mu M \pm 12$ (data not shown) comparable with the $K_d = 40\ \mu M \pm 4$ obtained in the displacement assay. The reversibility of the EO binding to sIR and the dependence of the interaction on an intact three-dimensional structure were established in separate experiments. First, the spectral differences resulting from bound EO disappear when the EO−sIR mixture is diluted to a ligand concentration lower than $0.1K_d$. Second, the differences also disappear when the spectra are collected in the presence of 6 M of the denaturant guanidine hydrochloride (data not shown).

Further spectroscopic characterization in solution was performed using mIR, and similar results were obtained in ER titrations of mIR followed by UV−vis spectroscopy. As shown in Figure 5A,B, the binding of ER to mIR is accompanied by a decrease in absorbance at 521 nm, an increase at 544 nm, and an isosbestic point at 533 nm. Although the spectral changes are rather small, the isosbestic point together with increases and decreases in absorbance are indicative of real differences. The change at 521 nm fits

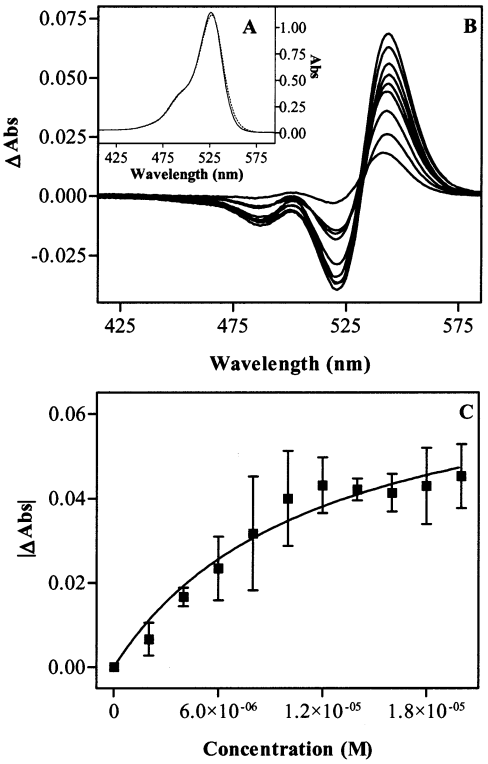

FIGURE 5: UV-vis spectroscopy of ER−mIR interaction. (A) Absorption spectrum of 20 μM ER in the absence (full line) and in the presence of 2 μM mIR (broken line). (B) Difference spectra between ER in the presence and absence of 2 μM mIR. Concentrations of ER in order of increasing difference at 543 nm are 2, 4, 6, 8, 10, 12, 14, 16, 18, and 20 μM. Conditions in panels A and B are 25 mM Tris, pH 7.8, 100 mM NaCl, 10 mM $MgCl_2$, 0.5 cm light path. (C) The absorption change at 521 nm versus [ER]. Full line is one-site binding equation (eq 2) fitted to the data points with $K_d = 11\ \mu M \pm 6$. All data points are mean of duplicate samples and shown with SEM bars.

eq 2 with $K_d = 11\ \mu M \pm 6$ (Figure 5C), equal to the 11 μM $\pm$ 1 obtained for ER binding to sIRFc in the displacement assay.

The binding of ER to mIR is accompanied by a small quench of ER fluorescence and a small red shift of the maximum emission wavelength (Figure 6A). An ER titration

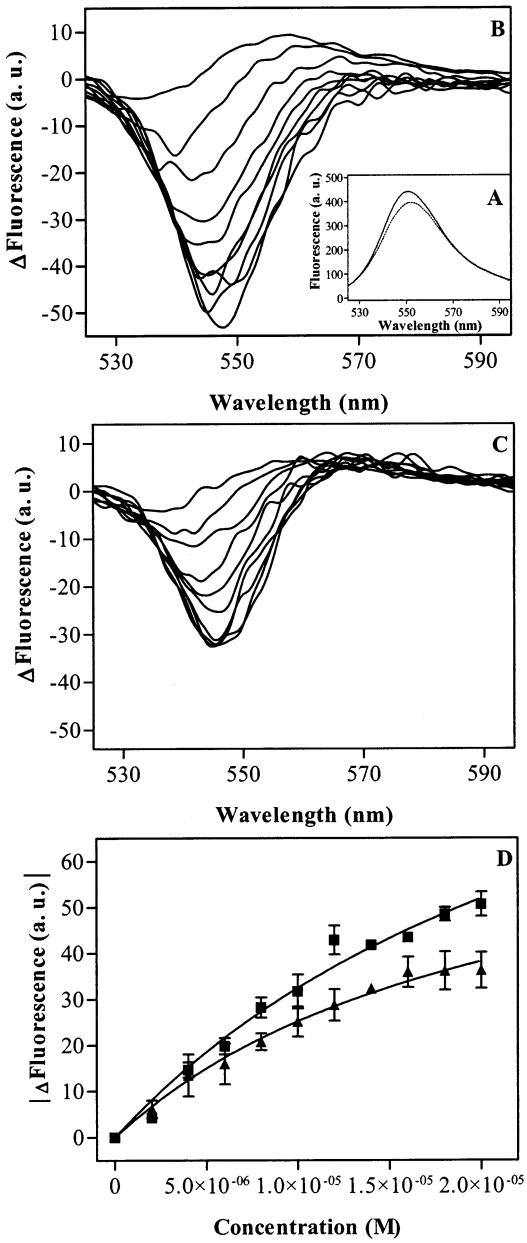

FIGURE 6: Fluorescence spectroscopy of ER−mIR interaction. (A) The emission spectrum of 20 μM ER alone (full line) and with 2 μM mIR (broken line) after excitation at 470 nm. (B) The difference emission spectra between concentrations of ER in the presence and absence of 2 μM mIR. Concentrations in order of decreasing fluorescence at 550 nm are as in Figure 5B. (C) Similar titration as in panel B but with 5 μM insulin HisB10Asp ProB28Asp added to the 2 μM mIR before the addition of ER. Conditions as in Figure 5. (D) The maximum quenching at each concentration versus the added [ER] for the titrations in B (■) and C (▲). Full lines are one-site binding equation (eq 2) with $K_d = 30\ \mu M \pm 8$ (■) and 22 μM ± 8 (▲). All data points are mean of duplicate samples and shown with SEM bars.

of mIR followed by fluorescence spectroscopy was performed both in the absence (Figure 6B) and presence of insulin HisB10Asp ProB28Asp (Figure 6C). Although the fluorescence change in the presence of insulin is significantly smaller, the binding of ER is not abolished by insulin, and similar K_d values are estimated in both cases (30 μM ± 8 and 22 μM ± 8, see Figure 6D). Similar results are obtained from a titration of sIR by ER monitored by fluorescence. Here, estimates of $K_d = 17\ \mu M \pm 4$ compared to the values of 11 μM ± 1 and 11 μM ± 6 were obtained using the

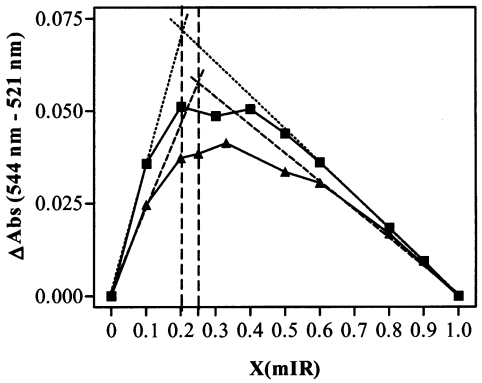

FIGURE 7: Job plot of the ER− mIR interaction. Total concentration of ER and mIR is 86 μM. Depicted is the difference between the two extremes at 544 and 521 nm in the difference absorption spectra between samples containing mIR and ER and samples only containing ER versus the mole fraction of mIR. Samples without insulin are shown as (■) and with 80 μM insulin HisB10Asp ProB28Asp present as (▲). Tangents to the two curves are drawn through $x = 0$ and $x = 1$. Indicated by vertical dashed lines are $x = 0.25$ (equals three ligands bound by each receptor molecule) and $x = 0.2$ (equals four ligands bound).

displacement assay and difference absorption spectroscopy, respectively (data not shown).

A characteristic feature of the spectroscopic measurements (Figures 4−6) is a failure to displace the spectroscopic change either by the addition of insulin or by preincubation of the receptor with insulin prior to ligand titration as would have been expected if the receptor sites for small molecule and insulin were overlapping as observed in the displacement assays (data not shown). The most reasonable explanation of this phenomenon is the existence of multiple small-molecule binding sites on the receptors with similar binding constants. To explore this possibility in detail, the binding stoichiometry of the interaction between ER and mIR both in the absence and presence of insulin was determined using the continuous variation method and difference absorption spectroscopy. The Job plots of the ER−mIR interaction are shown in Figure 7. Because the optimum of the Job plot is shifted to lower mole fraction of mIR than 0.5 both in the absence and presence of saturating insulin concentration, the binding interaction clearly involves more than one molecule of ER per molecule mIR. Although the signal is small, the data indeed indicate that four ER molecules are bound by mIR, while in the presence of insulin the stoichiometry is reduced to three. The shift in the optimum toward higher mIR mole fraction and the smaller ΔAbs signal in the presence of insulin are consistent with at least one bound ER molecule residing in or overlapping with the insulin binding site on mIR. This observation explains the apparent discrepancy between the displacement assay, where displacement of hormone from the intrinsic binding site is observed, and the spectroscopic titrations, where all binding phenomena with affinities in the same range are observed.

DISCUSSION

The approach described here utilizes the coordinates for a surface-exposed, functionally important epitope of the insulin molecule as a starting point for database searches. The approach led to the identification of TP, which displaces insulin from its receptor and is a weak stimulator of auto-

and substrate phosphorylation and glucose incorporation into lipid in the presence of insulin. Guided by further database searching, fluorescein and phenol red analogues were found to bind to the insulin receptor ligand binding domain. Although these hits elicit improved binding, they structurally diverge more than TP from the initial search query. Thus, the search and design strategy based on the coordinates of an isolated epitope is not sufficiently explored in the present study to clarify its usefulness.

It was not possible to optimize the weak insulin mimetic effects using closely related analogues of TP. Nevertheless, encouraged by the TP results, we characterized the interaction of fluorescein and phenol red analogues with the insulin receptor. Fluorescein and its derivatives structurally mimic nucleotides and are known to bind with micromolar affinities to proteins with ATP or other nucleotide binding sites (*41*−*46*). EO inhibits the autophosphorylation of hIR approximately 10 times stronger than it displaces insulin from sIRFc. This more potent antagonism toward hIR than sIRFc may reflect that these molecules also bind competitively to the ATP binding sites in the tyrosine kinase domains present in hIR but absent in the truncated sIRFc construct used in the displacement assay. Furthermore, fluorescein and its derivatives have recently been shown to bind to kinesin in a site different from the ATP binding site with affinities in the same range as presented here (*47*). Phenol red has been shown to interact with two receptors (*48*, *49*).

The appearance of transferred NOE cross-peaks and broader line widths in the NOESY spectrum of the EO−mIR mixture are distinct signatures of EO binding to mIR. The experiment (Figure 4) underscores the usefulness of transferred NOESY NMR spectra and line width broadening for screening purposes (*50*, *51*) and attest to the use of mIR as a screening target. Because only a small fraction of the total EO concentration is bound and because the short residence time in the bound state does not permit any chemical shift differences to be expressed, no such chemical shift differences are observed between the spectrum of free EO and that collected in the presence of mIR.

The changes in the UV−vis spectrum accompanying binding of EO and ER to sIR and mIR are similar to those observed when these molecules bind to other proteins (*52*−*54*) with small variations of the wavelengths at the extrema. Although EO has increased quantum yield in solutions with low polarity (*41*), the quenching of ER observed in the presence of sIR may originate from a number of different mechanisms. Indeed, the binding of fluorescein to bovine serum albumin is also accompanied by an emission quench (*55*).

It is remarkable that both UV−vis and fluorescence spectroscopy of the ligands show receptor induced changes with apparent K_d values essentially equal to those obtained in the displacement assay. The similar affinities obtained for binding to sIR and mIR in solution as compared to immobilized sIRFc are most easily explained by assuming that the same sites are being observed. However, the failure to displace bound small molecules either by addition of insulin or by preincubating receptors with insulin in the spectroscopic experiments suggests that more sites with incomplete overlap are involved.

The Job plot of the ER−mIR interaction confirms the presence of multiple binding sites. Since the spectroscopic titrations fit reasonably to a one-site binding equation, the four apparent ER sites must have K_d values so close that they appear as a single class of sites within experimental error. Of these four sites, one overlaps and competes directly with the insulin binding site on mIR and is responsible for the observed displacement of insulin by ER and its related molecules (Figure 3). The additional sites for small molecules apparently are noncompetitive with the binding of insulin. For the ER−mIR system, the receptor-induced changes in the ligand spectra are indeed smaller in the presence of insulin both in the fluorescence measurement (Figure 6) and the in Job plot (Figure 7). The lack of insulin effects on the transferred NOE cross-peaks in the EO NOESY spectrum (Figure 4) then originates from rather small differences between the various bound conformations of the rigid EO molecule leading to similar contributions from all bound forms.

The present work emphasizes at least two fundamental problems in the design of small molecule mimetics of peptide hormones. First, it appears that the contribution of the majority of the binding energy from the small functional epitope requires the context of its surrounding structural epitope. Without both being present, the necessary specificity is not available to fix the functional epitope in the productive, "hot" conformation. Second, a large protein surface already evolved for ligand binding appears to have a number of putative binding sites for a small molecule. The small size limits the possibilities for making specific interactions; hence, the molecule may bind a number of more or less similar sites with modest affinity.

In conclusion, the spectroscopic characterization uncovered a complexity in the small molecule−IR interaction that was not apparent from the single binding site interaction observed in the displacement assays. This result emphasizes the importance of a multidisciplinary approach in the validation of putative insulin mimetics in the absence of high-resolution structural information of the insulin receptor complexed with ligands. Finally, molecules such as erythrosine and iodophenol blue may serve as templates in the search for compounds that are more amenable for medicinal chemistry efforts.

ACKNOWLEDGMENT

We thank Elisabeth V. Andersen, Ane M. Blom, Susan E. Danielsen, Anne-Marie Kolstrup, and Birgitte Skjølstrup for excellent technical assistance; Lene Drube, Else Jost Jensen and Claus Kristensen for supply of receptor preparations; and Henning Thøgersen for valuable discussions.

REFERENCES

1. Wrighton, N. C., Farrell, F. X., Chang, R., Kashyap, A. K., Barbone, F. P., Mulcahy, L. S., Johnson, D. L., Barrett, R. W., Jolliffe, L. K., and Dower, W. J. (1996) *Science 273*, 458−464.
2. Cwirla, S. E., Balasubramanian, P., Duffin, D. J., Wagstrom, C. R., Gates, C. M., Singer, S. C., Davis, A. M., Tansik, R. L., Mattheakis, L. C., Boytos, C. M., Schatz, P. J., Baccanari, D. P., Wrighton, N. C., Barrett, R. W., and Dower, W. J. (1997) *Science 276*, 1696−1699.
3. Kimura, T., Kaburaki, H., Tsujino, T., Ikeda, Y., Kato, H., and Watanabe, Y. (1998) *FEBS Lett. 428*, 250−254.
4. Tian, S. S., Lamb, P., King, A. G., Miller, S. G., Kessler, L., Luengo, J. I., Averill, L., Johnson, R. K., Gleason, J. G., Pelus, L. M., Dillon, S. B., and Rosen, J. (1998) *Science 281*, 257−259.

5. Qureshi, S. A., Kim, R. M., Konteatis, Z., Biazzo, D. E., Motamedi, H., Rodrigues, R., Boice, J. A., Calaycay, J. R., Bednarek, M. A., Griffin, P., Gao, Y. D., Chapman, K., and Mark, D. F. (1999) *Proc. Natl. Acad. Sci. U.S.A. 96*, 12156−12161.
6. White, M. F., and Kahn, C. R. (1994) *J. Biol. Chem. 269*, 1−4.
7. Hubbard, S. R., Wei, L., Ellis, L., and Hendrickson, W. A. (1994) *Nature 372*, 746−754.
8. McDonald, N. Q., Murray-Rust, J., and Blundell, T. L. (1995) *Structure 3*, 1−6.
9. Schlein, M., Havelund, S., Kristensen, C., Dunn, M. F., and Kaarsholm, N. C. (2000) *J. Mol. Biol. 303*, 161−169.
10. Shechter, Y. and Karlish, S. J. (1980) *Nature 284*, 556−558.
11. Heyliger, C. E., Tahiliani, A. G., and McNeill, J. H. (1985) *Science 227*, 1474−1477.
12. Shaver, A., Ng, J. B., Hall, D. A., and Posner, B. I. (1995) *Mol. Cell. Biochem. 153*, 5−15.
13. Tamura, S., Fujita-Yamaguchi, Y., and Larner, J. (1983) *J. Biol. Chem. 258*, 14749−14752.
14. Leef, J. W., and Larner, J. (1987) *J. Biol. Chem. 262*, 14837−14842.
15. Steele-Perkins, G., and Roth, R. A. (1990) *J. Biol. Chem. 265*, 9458−9463.
16. Shiba, T., Tobe, K., Koshio, O., Yamamoto, R., Shibasaki, Y., Matsumoto, N., Toyoshima, S., Osawa, T., Akanuma, Y., Takaku, F., and Kasuga, M. (1990) *Biochem. J. 267*, 787−794.
17. Zhang, B., Salituro, G., Szalkowski, D., Li, Z., Zhang, Y., Royo, I., Vilella, D., Diez, M. T., Pelaez, F., Ruby, C., Kendall, R. L., Mao, X., Griffin, P., Calaycay, J., Zierath, J. R., Heck, J. V., Smith, R. G., and Moller, D. E. (1999) *Science 284*, 974−977.
18. Manchem, V. P., Goldfine, I. D., Kohanski, R. A., Cristobal, C. P., Lum, R. T., Schow, S. R., Shi, S. Y., Spevak, W. R., Laborde, E., Toavs, D. K., Villar, H. O., Wick, M. M., and Kozlowski, M. R. (2001) *Diabetes 50*, 824−830.
19. Baker, E. N., Blundell, T. L., Cutfield, J. F., Cutfield, S. M., Dodson, E. J., Dodson, G. G., Hodgkin, D. M., Hubbard, R. E., Isaacs, N. W., Reynolds, C. D., Sakabe, K., Sakabe, N., and Vijayan, N. M. (1988) *Philos. Trans. R. Soc. London B Biol. Sci. 319*, 369−456.
20. Ullrich, A., Bell, J. R., Chen, E. Y., Herrera, R., Petruzzelli, L. M., Dull, T. J., Gray, A., Coussens, L., Liao, Y. C., Tsubokawa, M., Manson, A., Seeburg, P. H., Grunfeld, C., Rosen, O. M., and Ramachandran, J. (1985) *Nature 313*, 756−761.
21. Sparrow, L. G., McKern, N. M., Gorman, J. J., Strike, P. M., Robinson, C. P., Bentley, J. D., and Ward, C. W. (1997) *J. Biol. Chem. 272*, 29460−29467.
22. Hubbard, S. R. (1997) *EMBO J. 16*, 5572−5581.
23. Garrett, T. P., McKern, N. M., Lou, M., Frenkel, M. J., Bentley, J. D., Lovrecz, G. O., Elleman, T. C., Cosgrove, L. J., and Ward, C. W. (1998) *Nature 394*, 395−399.
24. Ludvigsen, S., Roy, M., Thøgersen, H., and Kaarsholm, N. C. (1994) *Biochemistry 33*, 7998−8006.
25. Olsen, H. B., Ludvigsen, S., and Kaarsholm, N. C. (1996) *Biochemistry 35*, 8836−8845.
26. Ludvigsen, S., Olsen, H. B., and Kaarsholm, N. C. (1998) *J. Mol. Biol. 279*, 1−7.
27. Olsen, H. B., Ludvigsen, S., and Kaarsholm, N. C. (1998) *J. Mol. Biol. 284*, 477−488.
28. Wells, J. A. (1996) *Proc. Natl. Acad. Sci. U.S.A. 93*, 1−6.
29. Kraulis, P. J. (1991) *J. App. Crystallogr. 24*, 946−950.
30. Kristensen, C., Kjeldsen, T., Wiberg, F. C., Schäffer, L., Hach, M., Havelund, S., Bass, J., Steiner, D. F., and Andersen, A. S. (1997) *J. Biol. Chem. 272*, 12978−12983.
31. Kristensen, C., Wiberg, F. C., Schäffer, L., and Andersen, A. S. (1998) *J. Biol. Chem. 273*, 17780−17786.
32. Andersen, A. S., Kjeldsen, T., Wiberg, F. C., Christensen, P. M., Rasmussen, J. S., Norris, K., Møller, K. B., and Møller, N. P. (1990) *Biochemistry 29*, 7363−7366.
33. Cheng, Y., and Prusoff, W. H. (1973) *Biochem. Pharmacol. 22*, 3099−3108.
34. Moody, A. J., Stan, M. A., Stan, M., and Gliemann, J. (1974) *Horm. Metab. Res. 6*, 12−16.
35. Markussen, J., Halstrøm, J., Wiberg, F. C., and Schäffer, L. (1991) *J. Biol. Chem. 266*, 18814−18818.
36. Pace, C. N., Vajdos, F., Fee, L., Grimsley, G., and Gray, T. (1995) *Protein Sci. 4*, 2411−2423.
37. Hua, Q. X., Hu, S. Q., Jia, W. H., Chu, Y. C., Burke, G. T., Wang, S. H., Wang, R. Y., Katsoyannis, P. G., and Weiss, M. A. (1998) *J. Mol. Biol. 277*, 103−118 .
38. Job, P. (1928) *Ann. Chim. 9*, 113−134.
39. Musier, K. M., and Hammes, G. G. (1988) *Biochemistry 27*, 7015−7020.
40. Huang, C. Y. (1982) *Methods Enzymol. 87*, 509−525.
41. Skou, J. C., and Esmann, M. (1981) *Biochim. Biophys. Acta 647*, 232−240.
42. Gatto, C., and Milanick, M. A. (1993) *Am. J. Physiol. 264*, C1577−C1586.
43. Brand, L., Gohlke, J. R., and Rao, D. S. (1967) *Biochemistry 6*, 3510−3518.
44. Chiba, T., Sato, Y., and Suzuki, Y. (1987) *Biochim. Biophys. Acta 897*, 14−24.
45. Neslund, G. G., Miara, J. E., Kang, J. J., and Dahms, A. S. (1984) *Curr. Top. Cell. Regul. 24*, 447−469.
46. Majima, E., Yamaguchi, N., Chuman, H., Shinohara, Y., Ishida, M., Goto, S., and Terada, H. (1998) *Biochemistry 37*, 424−432.
47. Hopkins, S. C., Vale, R. D., and Kuntz, I. D. (2000) *Biochemistry 39*, 2805−2814.
48. Rajendran, K. G., Lopez, T., and Parikh, I. (1987) *Biochem. Biophys. Res. Commun. 142*, 724−731.
49. Greenberg, S. S., Johns, A., Kleha, J., Xie, J., Wang, Y., Bianchi, J., and Conley, K. (1994) *J. Pharmacol. Exp. Ther. 268*, 1352−1361.
50. Meyer, B., Weimar, T., and Peters, T. (1997) *Eur. J. Biochem. 246*, 705−709.
51. Moore, J. M. (1999) *Biopolymers 51*, 221−243.
52. Somerville, L. L., and Quiocho, F. A. (1977) *Biochim. Biophys. Acta 481*, 493−499.
53. Kalousek, I., Jandova, D., and Vodrazka, Z. (1978) *Eur. J. Biochem. 86*, 417−422.
54. Oikonomakos, N. G., Sotiroudis, T. G., and Evangelopoulos, A. E. (1979) *Biochem. J. 181*, 309−320.
55. Laurence, D. J. R. (1952) *Biochem. J. 51*, 168−180.

BI015672W